International Journal of Research and Review
[Indexed, Peer-Reviewed Journal]
Volume 13; Issue: 2; February 2026
Website: www.ijrrjournal.com
E-ISSN: 2349-9788; P-ISSN: 2454-2237

Research Paper

Benchmarking PHITS Simulations with XCOM for Photon Attenuation Analysis of Iron Portland Concrete

Meutia Rahmi Afifa[1], Pandji Triadyaksa[1], Ngurah Ayu Ketut Umiati[1], Fajar Arianto[1]

[1]Department of Physics, Diponegoro University, Semarang, Indonesia.

Corresponding Author: Meutia Rahmi Afifa

DOI: https://doi.org/10.52403/ijrr.20260241

ABSTRACT

This study evaluates photon attenuation characteristics of Iron-Portland (IP) concrete using Monte Carlo simulations with Particle Heavy Ion Transport System version 3.35 and benchmarks the mass attenuation coefficient results against XCOM calculations. Simulations were performed in the photon energy range of 0.06–0.16 MeV under narrow beam conditions. The PHITS results show good agreement with XCOM data, with relative deviations generally below 15%, confirming the reliability of PHITS for photon attenuation analysis. Based on the validated model, attenuation parameters including Mass Attenuation Coefficient, Linear Attenuation Coefficient, Half Value Layer, Mean Free Path, and Tenth Value Layer were evaluated for IP concrete and compared with ordinary concrete, aluminum, and copper. Iron-Portland concrete exhibits higher attenuation coefficients and lower shielding thickness parameters than ordinary concrete, indicating improved photon shielding performance due to its high iron content and density. The consistent trends among all attenuation parameters demonstrate the physical coherence of the simulation results and support the applicability of PHITS for radiation shielding evaluation of iron-based concrete materials.

Keywords: *Benchmark, Attenuation Coefficient, PHITS*

INTRODUCTION

Technological developments have led to increased use of ionizing radiation in various strategic sectors, including medicine, industry, and nuclear energy[1]. These developments have resulted in increased interaction between humans and the environment with sources of ionizing radiation, making radiation safety a crucial issue[2]. Ionizing radiation can be used in the medical world for diagnostic imaging and cancer treatment[3]. This radiation can be emitted in the form of electromagnetic waves or particles, originating from radioactive decay or controlled nuclear reactions[4][5]. Exposure to high doses of ionizing radiation or prolonged radiation exposure can cause various adverse health effects, thus requiring the strict application of radiation protection principles[6]. One of the main protection strategies is the use of effective shielding materials to reduce radiation intensity to safe levels[7]. However, the shielding performance of a material is influenced by several factors, including radiation energy, material density, and elemental composition [8][9]. Conventional gamma ray shielding materials such as lead are highly effective due to their high density, but their use is limited by toxicity, health hazards, and environmental concerns[10][11].

To overcome the limitations of traditional shielding materials, concrete has been widely used as an alternative radiation shielding material due to its flexibility, availability of raw materials, and relatively low production costs[1]. In medical facilities, concrete is often used in the construction of walls, floors, and ceilings of diagnostic scanning and radiotherapy rooms to ensure radiation safety[9]. The shielding performance of concrete can be improved by adding high-density aggregates such as barite, magnetite, and iron-based materials, which increase photon absorption and reduce the required shielding thickness[10][12]. The presence of elements with high atomic numbers (Z), including barium (Ba-56) and iron (Fe-26), increases the effective atomic number of the mixture and enhances photon absorption capacity [13].

In addition to natural aggregates, previous studies have explored the use of steel and iron waste to increase concrete density and radiation shielding performance [14]. Concrete with high iron content exhibits better mechanical properties, particularly compressive strength, due to stronger bonds between aggregates and cement [15][16]. Despite these advantages, systematic evaluation of concrete with very high iron content—such as Iron Portland Concrete—remains limited, especially in terms of quantitative radiation shielding parameters. Furthermore, although attenuation coefficients are often obtained from databases such as XCOM or simulated using Monte Carlo codes, comprehensive comparative studies between different simulation tools, particularly PHITS and XCOM, are still rare. This lack of comparative validation creates uncertainty in the reliability of simulation-based shielding assessments.

Therefore, this study aims to compare attenuation coefficient values obtained from Monte Carlo simulations with narrow beam geometry by comparing PHITS simulation results with XCOM data, using Iron Portland concrete as a high-density reference material. This study aims to evaluate the reliability of the Monte Carlo-based approach in radiation shielding analysis while providing deeper insights into the potential of iron-based concrete shielding for radiation protection applications.

MATERIALS & METHODS

The evaluation of radiation shielding characteristics in this study was conducted on Iron Portland concrete (IP), ordinary concrete (OC), and comparison materials in the form of aluminum (Al) and copper (Cu). The weight fractions of the constituent elements and the density of each material were obtained from the Compendium of Material Composition Data for Radiation Transport [17], which is the standard reference in radiation transport simulations. The material composition data is summarized in Table 1. IP concrete is classified as high-density concrete with a predominance of iron, while OC concrete is used as a representation of conventional concrete commonly applied in radiation facilities.

The protection parameters were calculated by modeling a monoenergetic photon source in the energy range of 0.06–0.15 MeV with an energy interval of 0.01 MeV. The modeling and simulation of photon radiation transport were performed using the Monte Carlo method with the Particle and Heavy Ion Transport code System (PHITS) version 3.28 software, which was developed and officially licensed by the Japan Atomic Energy Agency (JAEA) [18]. The simulation was run on a computer with an Intel(R) Core (TM) i7-10700 CPU @ 2.90 GHz processor, 8 GB RAM, and a 64-bit operating system.

The simulation was performed using a narrow beam geometry as shown in Figure 1 [19]. This geometry was designed to minimize the contribution of scattered radiation so that the attenuation coefficient obtained could be directly compared with theoretical data from XCOM. The monoenergetic photon source was modeled as an isotropic point source with a radius of 0.01 cm that emitted radiation in all directions. The test material was placed between the source and the detector, which were separated by a distance of 17.8 cm. The test material was modeled as a cylinder with a diameter of 4.5 cm and a thickness of 1 cm, and was placed at a distance of 8.3 cm from the source. The virtual detector is modeled as a sphere with a diameter of 0.564 cm and placed at a distance of 10.5 cm from the test material. The entire area around the beam path is surrounded by lead to absorb scattered radiation, while the narrow area between the source, material, and detector is defined as air.

Table 1. Composition of materials (weight fraction) used in the simulation

Component	IP Concrete	Ordinary Concrete	Aluminium	Copper
H	0.0033	0.022100	-	-
O	0.0586	0.574931	-	-
Mg	0.0013	0.001266	-	-
Al	0.0033	-	-	-
Si	0.0092	0.304627	-	-
S	0.0005	-	-	-
Mn	0.0035	-	-	-
Fe	0.8805	0.006435	-	-
Ca	0.0398	0.042951	-	-
C	-	0.002484	-	-
Na	-	0.015208	-	-
K	-	0.010045	-	-
Al	-	0.019953	1.00	-
Cu	-	-	-	1.00
Density	5.9 g/cm^3	2.3 g/cm^3	2.6989g/cm^3	8.96 g/cm^3

The PHITS input file in this study consists of several main parts, namely parameters, source, material, surface, cell, and tally [20]. The parameters section sets the number of particles and simulation output units, while the source section defines the characteristics of the isotropic monoenergetic photon source. The number of particle histories in this study is 1 × 10^9 histories. This is to ensure that the simulation results have low statistical uncertainty [21]. The cell section is defined based on a combination of material and surface to construct the overall simulation geometry. The photon flux calculation is performed using a t-track tally, which calculates the particle flux based on the path length per source divided by the cell volume. This tally is used to obtain the incident photon flux (φ_0) and transmission photon flux (φ) within the virtual detector cell. The photon intensity values without material and with material are then used in Lambert–Beer's law to calculate the material attenuation parameters [21].

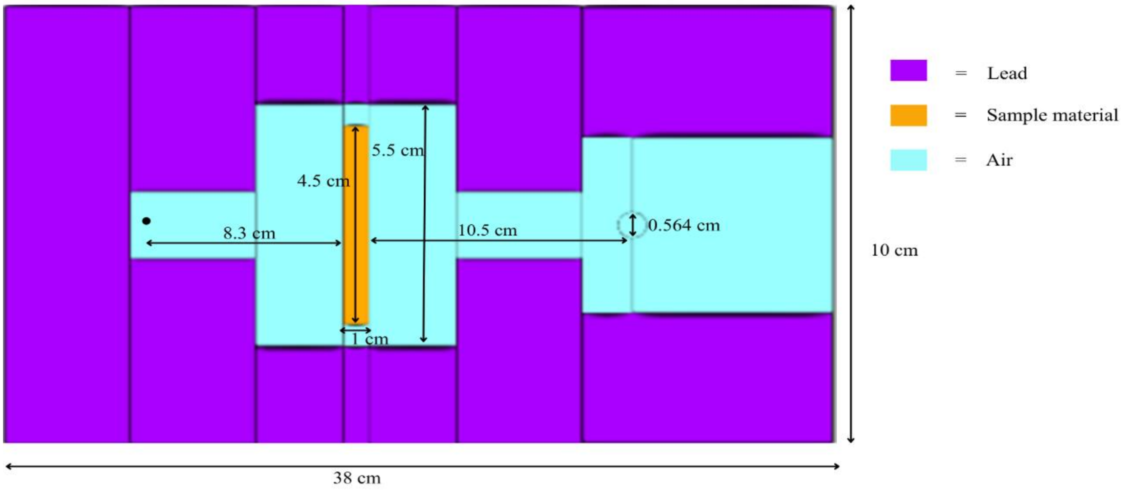

Figure 1. Narrow beam geometry used (Azzaoui et al, 2025).

The PHITS input file in this study consists of several main parts, namely parameters, source, material, surface, cell, and tally[20]. The parameters section sets the number of particles and simulation output units, while the source section defines the characteristics of the isotropic monoenergetic photon source. The number of particle histories in this study is 1×10^9 histories. This is to ensure that the simulation results have low statistical uncertainty[21]. The cell section is defined based on a combination of material and surface to construct the overall simulation geometry. The photon flux calculation is performed using a t-track tally, which calculates the particle flux based on the path length per source divided by the cell volume. This tally is used to obtain the incident photon flux (φ_0) and transmission photon flux (φ) within the virtual detector cell. The photon intensity values without material and with material are then used in Lambert–Beer's law to calculate the material attenuation parameters[21].

$$\mu(cm^{-1}) = \frac{1}{x} ln(\frac{\varphi_0}{\varphi}) \qquad (1)$$

Based on this linear attenuation coefficient, other radiation shielding characteristics can be calculated, such as the mass attenuation coefficient (MAC), Half Value Layer (HVL), Tenth Value Layer (TVL), and Mean Free Path (MFP). The mass attenuation coefficient (MAC) expresses the probability of photon interaction with material per unit mass and is calculated as:

$$\mu_m = \frac{\mu}{\rho} \qquad (2)$$

where I is the intensity of photons after penetrating the material, I_0 is the initial intensity, ρ is the density of the material, and x is the thickness of the material[22].

To benchmark XCOM results, the mass attenuation capability of a compound or mixture is determined by μ/ρ or the mass attenuation factor of the absorbing compound elements or shielding material.

$$\frac{\mu}{\rho} = \sum W_i (\frac{\mu}{\rho})_i \qquad (3)$$

where $W_i (\frac{\mu}{\rho})_i$ is the partial density and mass attenuation factor of the i-th constituent, and W_i is the weight fraction[23].

Other derivative parameters of LAC are used to evaluate the shield thickness calculated by the equations:

$$\mathrm{HVL(cm)} = \frac{ln(2)}{\mu} \qquad (4)$$

$$TVL(cm) = \frac{ln(10)}{\mu} \qquad (5)$$

$$MFP\ (cm) = \frac{1}{\mu} \qquad (6)$$

where μ is the LAC. HVL and TVL define the thickness of material required to reduce radiation intensity to 50% and 10%, respectively (Chang et al., 2023). Meanwhile, MFP represents the average distance traveled by photons before interacting with absorbing materials (Sopapan et al., 2023). To benchmark the PHITS simulation results, the MAC values obtained were compared with theoretical data from the XCOM database. This comparison is done to assess the consistency and reliability between the simulation code and theory, given that experimental evaluation cannot always be done directly. This difference is calculated using the equation

$$Dev(\%) = \left|\frac{\mu_{m\,XCOM} - \mu_{m\,PHITS}}{\mu_{m\,XCOM}}\right| x\ 100\% \qquad (7)$$

where $\mu_{m\,XCOM}$ is the result of the material attenuation coefficient from XCOM and $\mu_{m\,PHITS}$ is the result of the attenuation coefficient calculation from the PHITS simulation[21].

RESULT

The results of the mass attenuation coefficient (MAC) calculated by PHITS and XCOM are presented in Table 2. The calculations were performed at photon energies of 0.06–0.16 MeV. In general, the PHITS simulation results show good agreement with the XCOM theoretical calculations, with a relative deviation of less than 15% across the entire energy range.

The mass attenuation coefficient (μ/ρ) values for OC, IP, Al, and Cu materials in the 0.06–0.16 MeV energy range are shown in Figure 2. All materials show a decrease in μ/ρ values as the photon energy increases. Cu material has the highest μ/ρ value across all analyzed energies, followed by IP, while OC and Al show lower μ/ρ values. The difference in μ/ρ values between materials is most significant at low energies (< 0.10 MeV), while at higher energies the μ/ρ values of the four materials tend to converge.

Table 2. Comparison of mass attenuation coefficients between PHITS and XCOM and the percentage difference.

Energy (MeV)	**Ordinary Concrete**			**Iron-Portland**			**Al**			**Cu**		
	PHITS	**XCOM**	**%Dev**	**PHITS**	**XCOM**	**%Dev**	**PHITS**	**XCOM**	**%Dev**	**PHITS**	**XCOM**	**%Dev**
0.06	0.28	0.27	7%	1.10	1.11	0%	0.25	0.28	9%	1.37	1.59	14%
0.07	0.23	0.23	3%	0.75	0.76	1%	0.21	0.23	9%	0.98	1.06	7%
0.08	0.20	0.20	0%	0.54	0.55	3%	0.19	0.20	8%	0.71	0.76	7%
0.09	0.18	0.19	1%	0.41	0.43	4%	0.17	0.18	7%	0.54	0.58	6%
0.1	0.17	0.17	2%	0.33	0.35	5%	0.16	0.17	7%	0.43	0.46	7%
0.11	0.16	0.17	3%	0.28	0.30	6%	0.15	0.16	6%	0.35	0.38	8%
0.12	0.15	0.16	4%	0.24	0.26	6%	0.14	0.15	6%	0.29	0.32	8%
0.13	0.15	0.15	4%	0.21	0.23	7%	0.14	0.15	6%	0.25	0.28	8%
0.14	0.14	0.15	4%	0.19	0.21	7%	0.13	0.14	5%	0.23	0.25	8%
0.15	0.14	0.14	4%	0.18	0.19	7%	0.13	0.14	4%	0.20	0.22	8%
0.16	0.13	0.14	4%	0.17	0.18	7%	0.13	0.13	4%	0.19	0.20	8%

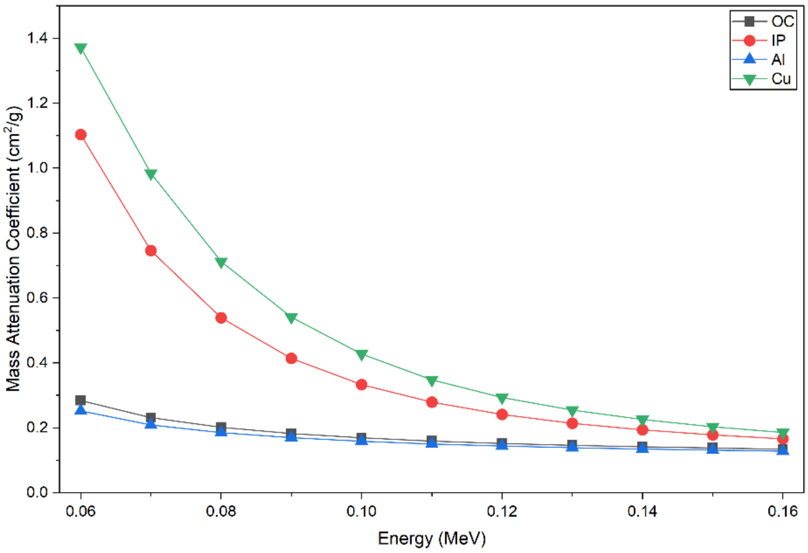

Figure 2. Mass Attenuation Coefficient of the tested materials

A similar trend is seen in the LAC values in Figure 3, which show differences in attenuation capacity with the contribution of material density. At low energies, the difference in attenuation capacity between copper, Portland Iron concrete, and regular concrete appears large, then decreases with increasing energy. Compared to the graph, at higher energies, the difference in attenuation capacity is still quite visible because the denser materials are able to interact and weaken photons.

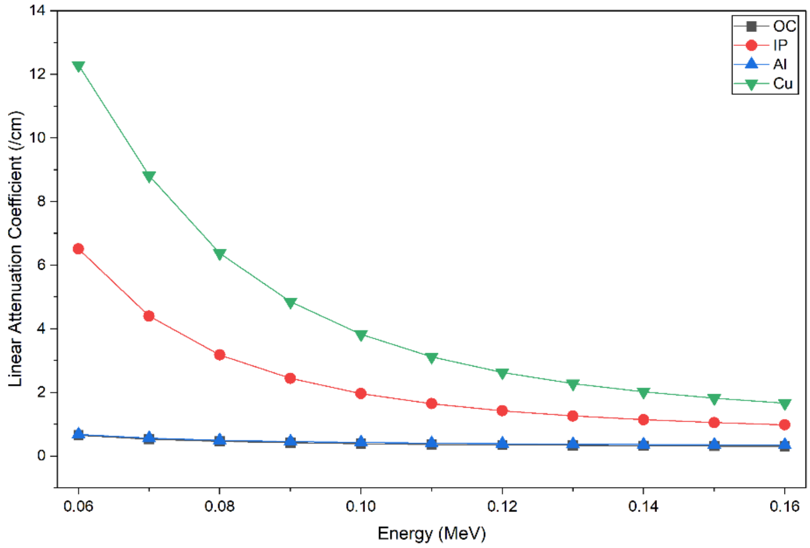

Figure 3. Linear Attenuation Coefficient of the tested materials

The HVL, MFP, and TVL values for OC, IP, Al, and Cu materials in the 0.06–0.16 MeV energy range are shown in Figures 4–6. All three parameters show an increasing trend with increasing photon energy for all materials. The OC and Al materials have the highest HVL, MFP, and TVL values across the entire energy range, while the IP and Cu materials show lower values. The thickness parameters (HVL and TVL) and average interaction distance (MFP) values for the IP material are consistently between those of Cu and OC, indicating better shielding characteristics than conventional concrete, but still below those of high-density metals.

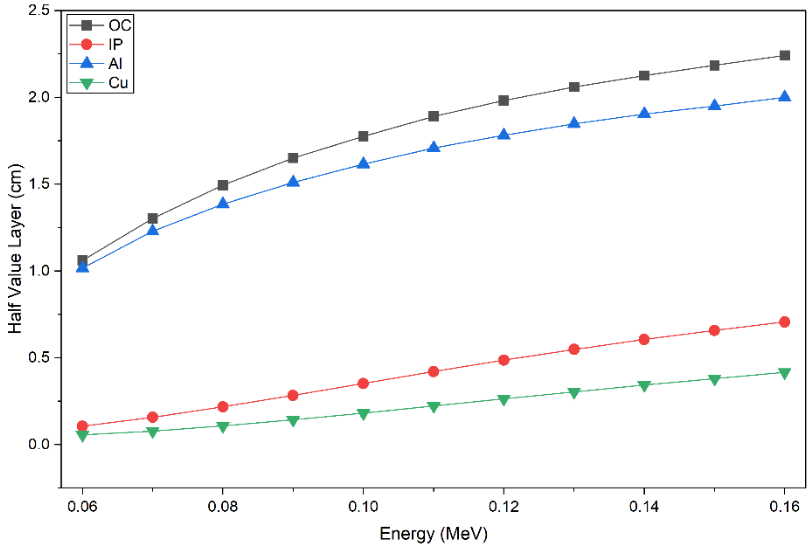

Figure 4. Half Value Layer values of materials tested in the study

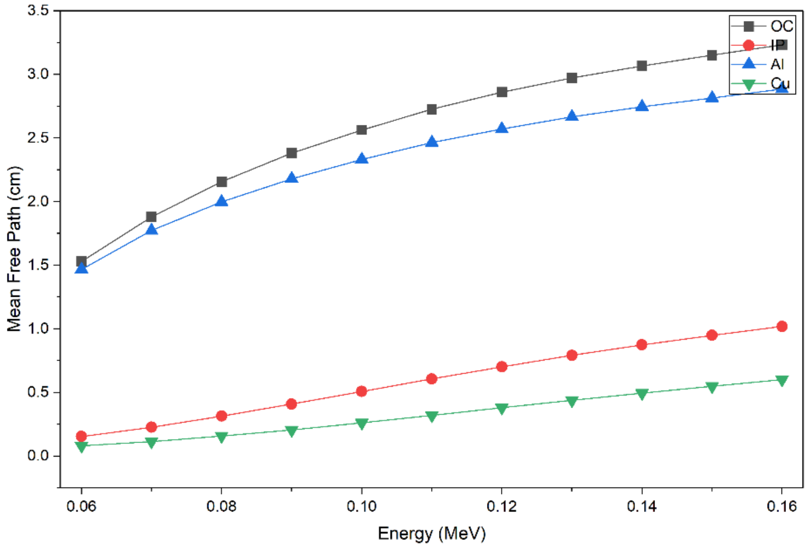

Figure 5. Mean Free Path values of materials tested in the study

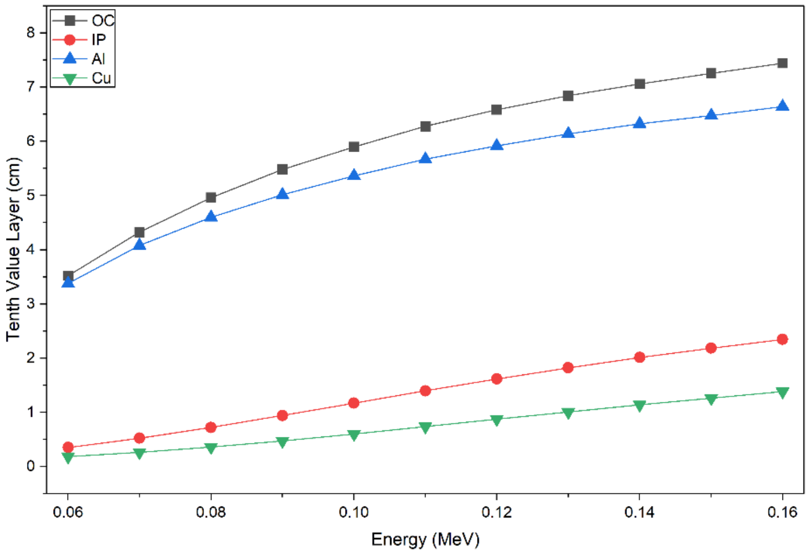

Figure 6. Tenth Value Layer values of materials tested in the study

The differences in values between materials are clearly visible across the entire energy range analyzed. This reflects the influence of density and elemental composition on photon attenuation capabilities.

DISCUSSION

Benchmarking of PHITS simulations against XCOM data was performed by comparing the mass attenuation coefficient (MAC) results with XCOM data. This data was obtained from the XCOM software developed by the National Institute of Standards and Technology (NIST). This data provides photon interaction data with theoretical mass attenuation coefficient calculations based on the formulation of the mixture of elements that make up a material [22]. In the XCOM software, the photon cross-section database used to determine μm is the NIST standard reference database, which was released in 2010 [24]. The comparison in Table 2 shows that the MAC values obtained from PHITS are consistent with the XCOM data in the photon energy range of 0.06–0.16 MeV, with a relative deviation of less than 15%. At higher energies, the deviation decreases to less than 10%. This shows that

PHITS can reproduce the photon attenuation behavior for homogeneous materials in narrow beam conditions. These differences may be caused by probabilistic processes [25]. The approach in the XCOM database is based on simulating an ideal situation of regular distribution in materials with standard geometry, rather than complex geometry [26]. However, the results of the study with an increase in photon energy from 0.06 to 0.16 MeV show a consistent downward trend in the mass attenuation coefficient (MAC) values for all materials analyzed.

The attenuation parameters for the materials are shown in Figures 2-6. Iron-Portland concrete consistently shows higher MAC and LAC values than ordinary concrete. In Figure 2, for low photon energies, such as 0.1 MeV, IP shows a much higher MAC (0.333 cm²/g) than OC (0.169 cm²/g). This clearly demonstrates better photon attenuation capability. This is due to the content of elements with high atomic numbers such as Fe. This high concentration of iron increases the probability of photon interaction with the material and enhances its shielding properties[13]. Although pure copper shows superior attenuation performance with a MAC at 0.1 MeV of 0.427 cm² due to its higher density and atomic number, the existence of Iron-Portland concrete offers a balance between protective effectiveness and practicality in radiation protection systems for construction.

Meanwhile, the linear attenuation coefficient value shows a correlation with density, with an increasing trend as the material density increases. This is in line with the research by [27], which emphasizes that concrete with a higher iron (Fe) concentration and greater density, such as Portland-Iron concrete, exhibits high attenuation. However, copper, which has a density of 8.96 g/cm³, has the best attenuation capability compared to all other materials tested. This is also due to the density and atomic number of the materials used. In general, the LAC value decreases with an increase in the radiation energy given. This is influenced by the interaction that occurs at different energy ranges. At low energies, photoelectric absorption is the dominant component[25]. This is evident from the correlation of the photoelectric cross section, which is highly dependent on photon energy and material atomic number [28][22]. However, at higher energies, Compton scattering becomes more common, showing a strong correlation with the electron density of the material and being less influenced by the atomic number. In this case, photoelectric absorption at high energies decreases, and the dominant interaction mechanism shifts from the photoelectric effect to less effective attenuation, namely Compton scattering [29].

The trends observed in HVL, MFP, and TVL values also support the attenuation capability demonstrated by LAC results. The HVL and TVL values are used to assess the effectiveness of materials in weakening radiation intensity. Specifically, Iron-Portland concrete is an example of a material used in the construction of radiation facilities. In Figure 4, the HVL value of Iron-Portland concrete is quite low at 0.106 cm for 0.06 MeV energy and 0.706 cm for 160 MeV energy. Meanwhile, the HVL value of ordinary concrete is 1.06 cm for 0.06 MeV energy and 2.24 cm for 160 MeV energy. This shows that concrete containing heavy metals, such as Iron-Portland, is more effective in reducing 50% of the incoming radiation intensity. Meanwhile, TVL shows similar results to HVL. Based on Figure 5, the TVL value of IP concrete is 0.354 cm for 0.06 MeV energy and 2.347 cm for 160 MeV energy. Meanwhile, the TVL value of ordinary concrete is 3.523 cm for 0.06 MeV energy and 7.445 cm for 0.160 MeV energy. However, pure copper has a higher ability to weaken radiation with a TVL value of 0.19 cm at an energy of 0.06 MeV and 1.383 cm at an energy of 0.16 MeV.

The decrease in LAC with increasing photon energy also causes an increase in the mean free path (MFP). If there are many photon interactions in a medium, the photons become weaker. Materials with shorter MFP are more effective in attenuating photons [30]. Concrete containing heavy metals provides a greater probability of interaction at short distances compared to concrete consisting of lighter elements [31][32][10]. Based on the results obtained, the MFP values show that Iron-Portland concrete has a lower MFP value than ordinary concrete, namely at an energy of 0.06 MeV with a value of 0.154 cm compared to ordinary concrete at 1.53 cm. At an energy of 0.160 MeV, the MFP value of IP concrete is 1.02 cm, which is lower than 3.23 cm for ordinary concrete. This indicates a greater probability of interaction occurring over a shorter distance. The three parameters HVL, MFP, and TVL, which depend on the attenuation coefficient, ultimately become a practical representation of attenuation behavior that is quantitatively described by the attenuation coefficient value.

The consistent attenuation characteristics observed in the MAC, LAC, HVL, MFP, and TVL parameters indicate that the simulation results consistently follow the exponential attenuation law for photon transport in matter. However, the analysis is limited to a relatively low photon energy range (0.06–0.16 MeV) and assumes a homogeneous material composition in a narrow beam geometry. These conditions do not account for microstructural heterogeneity or high-energy interaction mechanisms that become significant in practical shielding applications. Therefore, future work should extend the comparison to a wider energy range, incorporate additional Monte Carlo codes or experimental validation, and consider more complex geometric and material configurations.

CONCLUSION

This study was conducted to compare the photon attenuation coefficients obtained from PHITS simulations with XCOM data using Iron-Portland concrete as a high-density shielding material. The results show that the mass attenuation coefficients from PHITS are consistent with XCOM data in the photon energy range studied. Consistent trends in HVL, MFP, and TVL confirm the good gamma ray attenuation capability of Iron-Portland concrete. The agreement between simulation data and reference data demonstrates the validity of the Monte Carlo approach used in this study. Based on these results, Iron-Portland concrete can be considered an effective material for gamma radiation shielding applications. This study demonstrates that PHITS is a reliable tool for shield evaluation and provides a basis for future studies when experimental research is not yet possible or in more complex shield configurations.

Declaration by Authors

Acknowledgement: None

Source of Funding: None

Conflict of Interest: No conflicts of interest declared.

REFERENCES

1. Tekin HO, Sayyed MI, Issa SAM. Gamma radiation shielding properties of the hematite-serpentine concrete blended with WO3 and Bi2O3 micro and nano particles using MCNPX code. Radiat Phys Chem 2018; 150:95–100. https://doi.org/10.1016/j.radphyschem.2018.05.002.
2. Hashemi SA, Mousavi SM, Faghihi R, Arjmand M, Rahsepar M, Bahrani S, et al. Superior X-ray radiation shielding effectiveness of biocompatible polyaniline reinforced with hybrid graphene oxide-iron tungsten nitride flakes. Polymers (Basel) 2020; 12:1–21. https://doi.org/10.3390/polym12061407.
3. Jain S. Radiation in medical practice & health effects of radiation: Rationale, risks, and rewards 2021:1520–4. https://doi.org/10.4103/jfmpc.jfmpc.
4. Devi R, Poonamjot, Singh M, Sharma A. Efficacy of advanced concretes for attenuation of ionizing radiations: A comprehensive review and comparison. Prog Nucl Energy 2025; 178:105502. https://doi.org/10.1016/j.pnucene.2024.105502.
5. Karmaker N, Maraz KM, Islam F, Haque M, Mollah MZI. Fundamental characteristics and application of radiation 2021.
6. Pankaj G. The genomic effects of radiation exposure: induction of cancers and genetic aberrations in mammalian cells 2023; 27:112–22.

7. Al-Buriahi MS, Alomayrah N, Owoeye SS, Alsaiari NS. Effects of Er2O3 doping on the physical properties and gamma/neutron shielding performance of borate-tellurite glasses: PHITS Monte Carlo simulations. Radiat Phys Chem 2025;237. https://doi.org/10.1016/j.radphyschem.2025.113042.
8. Ali MAEM, Tawfic AF, Abdelgawad MA, Mahdy M, Omar A. Gamma and neutrons shielding using innovative fiber reinforced concrete. Prog Nucl Energy 2022;145. https://doi.org/10.1016/j.pnucene.2022.104133.
9. Onaizi AM, Amran M, Tang W, Betoush N, Alhassan M, Rashid RSM, et al. Radiation-shielding concrete: A review of materials, performance, and the impact of radiation on concrete properties. J Build Eng 2024;97. https://doi.org/10.1016/j.jobe.2024.110800.
10. Azreen NM, Rashid RSM, Mugahed Amran YH, Voo YL, Haniza M, Hairie M, et al. Simulation of ultra-high-performance concrete mixed with hematite and barite aggregates using Monte Carlo for dry cask storage. Constr Build Mater 2020; 263:120161. https://doi.org/10.1016/j.conbuildmat.2020.120161.
11. Khan MU, Ahmad S, Naqvi AA, Al-Gahtani HJ. Shielding performance of heavy-weight ultra-high-performance concrete against nuclear radiation. Prog Nucl Energy 2020; 130:103550. https://doi.org/10.1016/j.pnucene.2020.103550.
12. Rathore PS. Performance of High-Density Concrete with Iron Ores and Alumino Thermit Portion, As A Radioactive Barrier 2020;9:773–81.
13. Nabil IM, Samrah MG El, Omar A, Tawfic AF, Sayed AF El. Experimental, analytical, and simulation studies of modified concrete mix for radiation shielding in a mixed radiation field. Sci Rep 2023:1–16. https://doi.org/10.1038/s41598-023-44978-8.
14. Mironovs V, Korjakins A. POSSIBILITIES OF APPLICATION IRON CONTAINING WASTE MATERIALS 2011;26:14–9.
15. Sreeraj A, Francis N, Nadu T. INFLUENCE OF STEEL SHOTS IN ACHIEVING HIGH DENSITY CONCRETE 2018;9:1745–50.
16. Abduh N, Badrun B, Rahmadi A. Testing the Effect of Iron Casting Waste on Concrete Compressive Strength 2024;14:1354–62.
17. Detwiler R, McConn R, Grimes T, Upton S, Engel E. Compendium of Material Composition Data for Radiation Transport Modeling PNNL-15870 2021.
18. Sato T, Niita K, Matsuda N, Hashimoto S, Iwamoto Y, Furuta T, et al. Overview of particle and heavy ion transport code system PHITS. Ann Nucl Energy 2015;82:110–5. https://doi.org/10.1016/j.anucene.2014.08.023.
19. EL Azzaoui B, Kabach O, EL Abbari Y, Messous MY, Nabaoui K, Outayad R, et al. Assessment of radiation shielding properties for some concrete mixtures against photon and neutron radiations. Nucl Anal 2025:100152. https://doi.org/10.1016/j.nucana.2025.100152.
20. Koji N. User’ s Manual English version 2023.
21. El-Mesady IA, Hussein AE, Semary MM, Othman SM. Investigation of the mechanical properties, shielding parameters and flux distribution in borate - Based glass system using PHITS code; a simulation study. Opt Mater (Amst) 2023;138. https://doi.org/10.1016/j.optmat.2023.113699.
22. Sopapan P, Jaiboon O, Laopaiboon R, Yenchai C, Sriwunkum C, Issarapanacheewin S, et al. Determination of X-ray and gamma-ray shielding capabilities of recycled glass derived from deteriorated silica gel. Nucl Eng Technol 2023; 55:3441–9. https://doi.org/10.1016/j.net.2023.06.014.
23. Makkiabadi N, Ghiasi H. Monte Carlo Simulation and N-XCOM Software Calculation of the Neutron Shielding Parameters for the NCRP Report 144 Recommended Conventional Concretes. Front Biomed Technol 2024; 11:22–30. https://doi.org/10.18502/fbt.v11i1.14508.
24. Ozdogan H, Kilicoglu O, Akman F, Agar O. Comparison of Monte Carlo simulations and theoretical calculations of nuclear shielding characteristics of various borate glasses including Bi, V, Fe, and Cd. Appl Radiat Isot 2022; 189:110454. https://doi.org/10.1016/j.apradiso.2022.110454.
25. Shirmardi SP, Shamsaei M, Naserpour M. Comparison of photon attenuation

coefficients of various barite concretes and lead by MCNP code, XCOM and experimental data. Ann Nucl Energy 2013; 55:288–91. https://doi.org/10.1016/j.anucene.2013.01.002.

26. Yu L, Pereira ALC, Tran DNH, Santos AMC, Losic D. Bismuth Oxide Films for X-ray shielding: Effects of particle size and structural morphology. Mater Chem Phys 2021;260. https://doi.org/10.1016/j.matchemphys.2020.124084.
27. Mesbahi A, Azarpeyvand AA, Khosravi HR. Does concrete composition affect photoneutron production inside radiation therapy bunkers? Jpn J Radiol 2012; 30:162–6. https://doi.org/10.1007/s11604-011-0030-y.
28. Tekin HO, Susoy G, Issa SAM, Ene A, Almisned G, Rammah YS, et al. Heavy metal oxide (HMO) glasses as an effective member of glass shield family: A comprehensive characterization on gamma ray shielding properties of various structures. J Mater Res Technol 2022; 18:231–44. https://doi.org/10.1016/j.jmrt.2022.02.074.
29. Pianpanit T, Saenboonruang K. High-Energy Photon Attenuation Properties of Lead-Free and Self-Healing Poly (Vinyl Alcohol) (PVA) Hydrogels: Numerical Determination and Simulation. Gels 2022;8. https://doi.org/10.3390/gels8040197.
30. Samdani M, Basha B, Alsufyani SJ, Kebaili I, Sekhar KC, Alrowaili ZA, et al. Gamma shielding performance of B2O3/BaO-based glassy system: Synthesis and simulation study. Radiat Phys Chem 2024;214. https://doi.org/10.1016/j.radphyschem.2023.111301.
31. Alghamdi AAA. MCNPX Estimation of Photoneutron Dose to Eye Voxel Anthropomorphic Phantom From 18 MV Linear Accelerator. Dose-Response 2023; 21:1–7. https://doi.org/10.1177/15593258231169807.
32. Oto B, Gür A, Kavaz E, Çak T, Yaltay N. Progress in Nuclear Energy Determination of gamma and fast neutron shielding parameters of magnetite concretes 2016;92. https://doi.org/10.1016/j.pnucene.2016.06.011.

How to cite this article: Meutia Rahmi Afifa, Pandji Triadyaksa, Ngurah Ayu Ketut Umiati, Fajar Arianto. Benchmarking PHITS simulations with XCOM for photon attenuation analysis of Iron Portland concrete. *International Journal of Research and Review*. 2026; 13(2): 429-439. DOI: *https://doi.org/10.52403/ijrr.20260241*

******